Table 3.14

Survey of the C_2 olefin selectivity and the ethene mole fraction for both FeRu/SiO_2 and potassium promoted fused iron (C73) at 250°C and various pressures.

Catalyst	Exp. no.	H.O.S.	Flow in 1)	X_{CO} [%]	p_{H_2} [bar]	p_{CO} [bar]	P [bar]	$p_{C_2H_4}$ [bar]	C_2 Ol.sel. [%]	$\frac{p_{C_2H_4}}{p_{C_1}-C_4}$ [-]
RuFe/SiO_2	14.25	839	235	12.6	0.92	0.39	1.4	3.2E-4	31.4	0.041
Fe	16.08	242	98	28.1	1.09	0.33	1.5	25.0E-4	71.4	0.136
RuFe/SiO_2	14.16	574	206	9.1	3.78	5.05	9.0	2.8E-3	31.0	0.031
Fe	16.24	692	205	26.8	2.40	5.78	9.0	16.3E-3	84.8	0.221
RuFe/SiO_2	14.11	406	207	13.5	10.78	5.03	17.0	2.7E-3	19.9	0.014
Fe	13.17	240	318	64.0	5.65	6.02	17.0	100.6E-3	61.1	0.150

1) ml(20°C and 1 bar)/min

3.3.11 The olefin selectivity observed with other bimetallic catalysts

Besides RuFe other combinations with iron has been developed as well. Below the performance of a few catalysts in respect of the olefin selectivity is compared with that of RuFe and promoted fused iron

The properties of the catalysts are summarized in Table 3.15. Considering PdFe/ZnO and CoFe/SiO_2 it can be concluded that Pd and Co addition lowers the olefin selectivity despite the very low conversion. The value of the olefin selectivity is of the same order of magnitude as that obtained for RuFe/SiO_2 but much lower than that for fused iron as shown in Table 3.15. At a higher conversion iron promoted with copper produces predominantly paraffins

The addition of manganese differs from that of ruthenium, copper, cobalt and palladium because manganese lowers the activity [21]. Diffenbach et al. [22], Lehmann et al.[23], and Kölbel and Tillmetz [24] report that MnFe catalysts with a high manganese content produce hydrocarbons with a high

C_2-C_4 fraction which predominantly contains olefins. However, when the performance of these MnFe catalysts (results of other investigators [21,25,26,27] included) are compared with that of the iron catalyst used in this study, it can be concluded that the latter produces low hydrocarbons with a higher olefin content. Secondary hydrogenation appear to be more significant with MnFe catalysts [21,25,26,28] which may be attributed to the higher reactor temperature used with MnFe (see Table 3.15). This higher temperature is necessary to achieve a sufficiently high activity.

Finally, it may be concluded that the addition of potassium to iron is much more succesful to obtain a catalyst which produces hydrocarbons with a high olefin content than the addition of Co, Cu, Pd, Ru or Mn.

Table 3.15

Comparison of the olefin selectivity obtained with various catalysts

Catalyst	T [°C]	P [bar]	$(H_2/CO)_{in}$ [mol/mol]	X_{CO} [%]	Olefin s. [%]	Ref.
3.5 wt%PdFe(1:4.8)/ZnO	300	6.8	1.0	<5	45 (C_2)	29
2.5 wt%Fe/ZnO	300	6.8	1.0	<5	67 (C_2)	29
4.9 wt%CoFe(1:4.0)/SiO_2	250	13.6	3.7	9	18 (C_2)	30
4.9 wt%Fe/SiO_2	250	13.6	3.7	6	28 (C_2)	30
5.0 wt%RuFe/SiO_2	230	9.0	1.0	14	29 (C_2)	31
CuFe(1:19)	250	-	-	71 [1)]	28 (C_2-C_4)	21
Fused iron	250	9.0	0.7	74 [1)]	71 (C_2-C_4)	32
MnFe(9.6:1)	275	13.6	1.0	18	60 (C_2-C_4)	26
Fused iron	250	13.6	1.0	17	81 (C_2-C_4)	26

1) Conversion of H_2+CO

3.3.12 Mössbauer analysis

3.3.12.1 Introduction

From the Fischer-Tropsch synthesis experiments carried out with both $RuFe/SiO_2$ and Ru/SiO_2, it has become clear that the catalytic performance of $RuFe/SiO_2$ does not differ significantly from the performance of Ru/SiO_2. Therefore it is likely that the active surface of these catalysts is similar. This would indicate that the bimetallic character has disappeared under the reaction conditions used in this study. This bimetallic character of $RuFe/SiO_2$ is responsible for the different activity and selectivity of RuFe catalysts according to various reports [1,2,3,4,8] with respect to monometallic Ru and Fe catalysts. However, these reports are mostly based on measurements at atmospheric pressure and only after a short time on stream. Therefore, the existence of the bimetallic phase of a used $RuFe/SiO_2$ was analyzed by means of Mössbauer measurements after the catalyst had been exposed to a high pressure during a few days on stream. This Mössbauer analysis was compared with that of a fresh $RuFe/SiO_2$ catalyst and a sample which had been exposed to synthesis gas for only 3 hours at atmospheric pressure.

3.3.12.2 Experimental

Three samples 5.0 wt% RuFe (1:3)/SiO_2 were prepared and reduced with hydrogen in accordance with the procedure described in section 3.2.1. The first sample was reduced without any further treatment; it is used as reference. The second sample (0.5 g) was exposed to synthesis gas in a conventional down flow fixed-bed reactor for a short time, as described by Sommen et al.[12].

The reaction conditions are reported in Table 3.16. The third sample was pretreated with $CO+H_2$ in a high pressure down flow fixed-bed reactor as described by Stoop [3]. The reaction conditions are also reported in Table 3.16. From these three samples Mössbauer spectra were recorded. These experiments were performed and interpreted by A.M. van der Kraan and E. Gerkema at the "Interuniversitair Reactor Instituut" in Delft.

Table 3.16

Reaction conditions of the pretreatment of sample 2 and 3

Sample	Temperature [°C]	Pressure [bar]	Flow [ml/min] 1)	H_2/CO [mol/mol]
2	275	1	180	2
3	275	31 (1 day)	180	2
		21 (3 days)		
		11 (1 day)		
		1 (1 day)		

1) measured at 20°C and 1 bar

3.3.12.3 Results and discussion

The spectra of the samples mentioned are shown in Figure 3.22. The spectra of sample 1 and 2 are similar. These spectra suggest the absence of iron carbides. This should mean that the catalyst is still completely bimetallic after 3 hours on stream. However, the spectrum of sample 3 significantly differs from that of the other two samples. The Mössbauer spectrum of sample 3 indicates that $RuFe(1:3)/SiO_2$ is carburized completely after 144 hours on stream. The carbides have been characterized as χ-Fe_5C_2 and an iron carbide phase which consists of small particles with supermagnetic performance [13]. The complete carburization of the iron implies that Ru and Fe completely segregated either before or during to the carburization process. Thus, these results clearly show that bimetallic $RuFe(1:3)/SiO_2$ is not stable during the Fischer-Tropsch synthesis at a moderate temperature and high pressure. The presence of a small amount of iron carbide together with the metallic component for $RuFe(4.8:1)/SiO_2$ after having been kept in a $2H_2/CO$ mixture at 570 K and atmospheric pressure for only 38 hours [14], suggests the instability of bimetallic RuFe on a silica carrier even at atmospheric pressure. Therefore, it is likely, that the decomposition of the bimetallic particles starts immediately after contact with CO and H_2. The extent of decomposition depends on the time on stream and the rate of

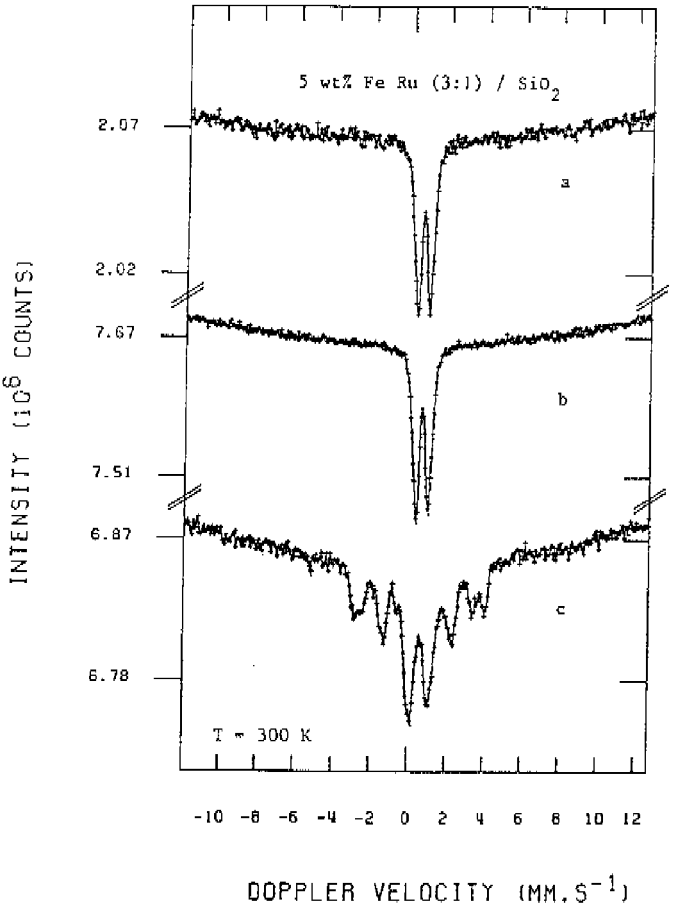

Fig. 3.22 Mössbauer spectra of 5 wt% RuFe(1:3)/SiO_2.
Sample 1: only reduced
2: after 3 hours on stream at atmospheric pressure
3: after 6 days on stream at high pressure

decomposition which, in turn, depends on the reaction conditions.As could be expected, this rate increases with increasing temperature, pressure, synthesis gas conversion level (water vapour pressure!) and iron to ruthenium ratio.

Unfortunately, these conditions prevent the commercial application of this type of catalyst for the synthesis gas conversion via the Fischer-Tropsch route.

3.4 Discussion

During the first hours on stream, the production of a Ru/SiO_2 catalyst, freshly reduced with hydrogen, mainly consists of methane. This is probably due to a high surface coverage by hydrogen as is indicated by the high value of the H_2 chemisorption [3]. The product distribution and the course of the activity is noticeably influenced by the addition of Fe to Ru. In contrast with Ru/SiO_2, the methane selectivity over fresh $RuFe(1:3)/SiO_2$ is relatively low but it increases rapidly as time goes on, along with the deactivation of the catalyst. The initial activity of $RuFe/SiO_2$ is much lower than that of Ru/SiO_2. This can also be explained by the lower H_2 coverage of an iron containing metal surface with respect to pure ruthenium [3].

Nevertheless, the very low olefin selectivity obtained with fresh $RuFe/SiO_2$ at a high pressure and a low CO conversion level indicates that the hydrogenation activity is still much too high to prevent secondary hydrogenation of olefins.

The results reported here have shown that the olefin selectivity drops extremely rapidly as the conversion increases. Secondary hydrogenation is already important at a 0.1% conversion level! This explains why such low selectivities are found at elevated pressure, relative to satisfying values at atmospheric pressure. It may also explain the selectivity difference between the Ru/SiO_2 catalyst and the much less active $FeRu/SiO_2$ catalyst.

Contrary to the initial period, the performance of $RuFe/SiO_2$ is similar to that of Ru/SiO_2 after only one day on stream. The activity, the product distribution and the olefin selectivity are hardly distinguishable. It appears that the properties of $RuFe/SiO_2$ are eventually determined by the Ru atoms alone, unaffected by the presence

of Fe. The absence of a close contact between the Ru and Fe atoms is supported by Mössbauer analysis which indicates that Ru and Fe are segregated after a few days on stream at a high pressure. The segregation is probably accellerated by the carburization of Fe, which is thermodynamically favoured by higher CO pressures.

The olefin selectivity of $RuFe/SiO_2$ is very low relative to that of fused iron, particularly when the comparison is made after sometime on stream. The selectivity decreases extremely rapidly with increasing olefin/CO pressure ratio. Moreover, it appears that the hydrogen pressure strongly influences this selectivity, indicating that a simple competition model as described in Chapter 2 does not apply here. Apparently, the pressure of H_2 promotes the formation of paraffins either by an increase of the secondary hydrogenation or by an increase of the formation of paraffins directly from synthesis gas.

The low steady-state activity of $RuFe/SiO_2$ and Ru/SiO_2 is partly caused by the very strong inhibition by water. The CO conversion has to be below 1% for it to prevent the inhibition of the hydrocarbon synthesis by water. The product distribution is not significantly influenced by the water pressure, indicating that water does not occupy specific reaction sites.

Summarizing, it can be concluded that the addition of Fe to Ru supported on silica is only effective during the first hours on stream. The instability of the bimetallic RuFe particles under Fischer-Tropsch conditions results in the formation of a mixture of active Ru particles with inactive iron carbides with properties similar to a normal Ru/SiO_2 catalyst.

Appendix 1

Model I

According to Kellner and Bell [20] the kinetics of hydrocarbon synthesis over Ruthenium catalysts can be derived from the following reactions:

1. $CO + * \underset{k_{-1}}{\overset{k_1}{\rightleftharpoons}} CO*$	θ_{CO}	$= K_1 P_{CO} \theta_v$
2. $CO* + * \underset{k_{-2}}{\overset{k_2}{\rightleftharpoons}} C* + O*$	$\theta_C \theta_O$	$= K_2 \theta_{CO} \theta_v$
3. $H_2 + 2* \underset{k_{-3}}{\overset{k_3}{\rightleftharpoons}} 2H*$	θ_H	$= (K_3 P_{H_2})^{1/2}$
4. $O* + H_2 \overset{k_4}{\rightarrow} H_2O + *$	r_{H_2O}	$= K_4 \theta_O p_{H_2}$
5. $C* + H* \underset{k_{-5}}{\overset{k_5}{\rightleftharpoons}} CH* + *$	$\theta_{CH} \theta_v$	$= K_5 \theta_C \theta_H$
6. $CH* + H* \underset{k_{-6}}{\overset{k_6}{\rightleftharpoons}} CH_2* + *$	$\theta_{CH_2}\theta_V$	$= K_6\theta_{CH} \theta_H$
7 $CH_2* + H* \underset{k_{-7}}{\overset{k_7}{\rightleftharpoons}} CH_3*+ *$	$\theta_{CH_3}\theta_V$	$= K_7\theta_{CH_2}\theta_H$
8. $CH_3* + H* \overset{k_8}{\rightarrow} CH_4 + 2*$	r_{CH_4}	$= K_8\theta_{CH_3}\theta_H$
9. $CH_3* + CH_2* \overset{k_9}{\rightarrow} C_2H_5* + *$	$r_{C_2H_5}$	$= K_9\theta_{CH_3}\theta_{CH_2}$
10. $C_2H_5* + * \overset{k_{10}}{\rightarrow} C_2H_4 + H* + *$	$r_{C_2H_4}$	$= K_{10}\theta_{C_2H_5} \theta_v$
11. $C_2H_5* + H* \overset{k_{11}}{\rightarrow} C_2H_6 + 2*$	$r_{C_2H_6}$	$= K_{11}\theta_{C_2H_5} \theta_H$
12. $C_2H_5* + CH_2* \overset{k_{12}}{\rightarrow} C_3H_7* + *$	$r_{C_3H_7}$	$= K_{12}\theta_{C_2H_5} \theta_{CH_2}$

(θ_v is the fraction of active sites which is not occupied)

They suppose that the catalyst surface is saturated by CO at a low conversion level. However, it is clear from the experiments presented in Table 3.10 that the influence of water will have to be considered. Therefore it is supposed that water can absorb on the active sites and inhibites the rate of synthesis gas conversion:

$$H_2O + * \rightleftharpoons H_2O* \tag{13}$$

It is supposed further that the rate determing step (RDS) is the hydrogenation of a CH_x intermediate:

$$CH_x* + H* \overset{RDS}{\rightleftharpoons} CH_{x+1} + * \tag{14}$$

The formation of water via a sequence of Langmuir-Hinshelwood steps is more likely than a Rideal-Eley step. Therefore equation (4) is replaced by

$$O* + H* \rightarrow OH* + * \tag{4.1}$$

$$OH* + H* \rightarrow H_2O + 2* \tag{4.2}$$

The rate determining step can be written as:

$$r_{CO+H_2} = k\, \theta_{CH_x}\, \theta_H \tag{15}$$

which can be expressed as

$$r_{CO+H_2} = k'\, p_{CO}^{\frac{1}{2}}\, p_{H_2}^{\frac{1}{2}(x+1)} \theta_v^{\,2} \tag{16}$$

whereby it is estimated that $k_6 \gg k_{-6}$ and $k_{41} \gg k_{-41}$
If CO, C* and H_2O* are the most abundant surface species equation (16) can be written as

$$r_{CO+H_2} = \frac{k'\, p_{CO}^{\frac{1}{2}}\, p_{H_2}^{\frac{1}{2}(x+1)}\, K_1K_2k_{4.1}/k_5\, K_3^{\frac{1}{2}(x+1)}}{\left[1 + K_1P_{CO} + \frac{k_{4.1}K_1K_2P_{CO}^{\frac{1}{2}}}{k_5} + \frac{p_{H_2O}}{K_{13}}\right]^2} \tag{17}$$

with $k' = k_5,\ k_5k_6,\ k_5k_6k_7$ for $x = 0,1,2$ respectively.

Model II

This model is similar to model I but the reactions 4.1 and 4.2, the hydrogenation of surface oxygen and surface hydroxide, are estimated to be equilibrium reactions. This results in:

$$r_{CO+H_2} = \frac{k'(K_1K_2K_3K_{4.1}K_{4.2}\,K_3^{\frac{1}{2}(x+1)}/K_{13})(p_{CO}p_{H_2}/p_{H_2O})p_{H_2}^{\frac{1}{2}(x+1)}}{\left[1 + K_1p_{CO} + \frac{K_1K_2K_3K_{4.1}K_{4.2}}{K_{13}} \cdot \frac{p_{CO}p_{H_2}}{p_{H_2O}} + K_{13}p_{H_2O}\right]^2} \qquad (18)$$

References

1 Vannice, M.A.; Lam, Y.L.; Garten, R.L., Adv. Chem., 178 (1979) 25-34

2 Vannice, M.A.; Lam, Y.L.; Garten, R.L., ACS Petrol. Div., Preprints, 23 (1978) 495-501

3 Stoop, F., Ph.D. Thesis, Eindhoven University of Technology (1986)

4 Stoop, F.; Wiele, K. van der, Appl. Catalysis, 23 (1986) 35-47

5 Fleisch, T.; Delgass, W.N.; Winograd, N., Surf. Interfase Anal., 3, 1 (1981) 23-28

6 Aschenbeck, D.P., Ph.D. Thesis, Purdue University, West Lafeyette, IN US (1979)

7 Lazar, K.; Schay, Z.; Guczi, L., J. Mol. Cat., 17 (1982) 205-218

8 Guczi, L., Catal. Rev.-Sci. Eng., 23, 3 (1981) 329-376

9 Lazar, K.; Reiff, W.M.; Mörke, W.; Guczi, L., J. Catal., 100 (1986) 118-129

10 Ott, G.L.; Fleisch, T.; Delgass, W.N., J. Catal., 60 (1979) 394-403

11 Schay, Z.; Guczi, L., React. Kinet. Catal. Lett., 14 (1980) 207-212

12 Sommen, A.B.P.; Stoop, F.; Wiele, K. van der, J. Appl. Catal., 14 (1985) 277

13 Kraan, A.M. van der, personal communication

14 Lazar, K.; Reiff, W.M.; Guczi, L., Hyperfine Interactions, 28 (1986) 871-874

15 Berry, F.J.;Liwu, L.; Chengyu, W.; Renyan, T.; Su, Z.; Dongbai, L., J. Chem. Soc., Faraday Trans.,1 (1985) 2293-2305

16 Huff, G.A. Jr. and Satterfield, C.N., Ind. Eng. Chem. Process Des. Dev., 23 (1984) 696-705

17 Anderson, R.B.; Karn, F.S.; Schulz, J.F., Bull. - U.S. Bur. Mines, 614 (1964) 46

18 Dry, M.E., Ind. Eng. Chem., Prod. Res. Dev., 15 (1976) 282-286

19 Dixit, R.S. and Tavlarides, L.L., Ind. Eng. Chem. Process Des. Dev., 22 (1983) 1-9

20 Kellner, C.S.; Bell, A.T., J. Catal., 67 (1981) 175-185

21 Deckwer, W-D., in "Mass Transfer in Chemical Reaction in Multiphase Systems, Vol II: Three Phases Systems, Alper, E. (Ed.), NATO ASI Series, p 287-349 (1983) Martinus Nijhoff Publishers, The Hague

22 Diffenbach, R.A.; Faulth, D.J.; Schehl, R.R., Paper no. 40b, presented at AIChE Meeting, Detroit, Mich., August (1981)

23 Lehmann, H.J.; Ralek, M.; Deckwer, W-D., Paper no. 103d, presented at 73rd Annual Meeting AIChE, Chicago, Nov. (1980)

24 Kölbel, H.; Tillmetz, K.D., DE 2507647 (1976)

25 Satterfield, C.N.; Stenger, H.G., I.E.C. Proc. Des. Dev.,23 (1984) 26

26 Pennline, H.W.; Zarochak, M.F.; Tischer, R.E.; Schehl, R.R., Appl. Cat., 21 (1986) 313-328

27 Malessa, R.; Baerns, M., I.E.C. Res., 27 (1988) 279-283

28 Mohammed, M.S.; Schmidt, B.; Schneidt, D.; Ralek, M., Chem.-Ing.-Tech., 51 (1979) 739-741

29 Gustafson, B.L.;Wehner, P.S., Prep. Pap.-A.C.S. Div. Fuel Chem., 31 (1986) 109-115

30 Butt, J.B.; Schwartz, L.H.; Baerns, M.; Malessa, R., I.E.C. Prod. Res. Dev., 23 (1984) 51-56

31 This study, Chapter 3 :Run 1, Experiment no 2

32 This study, Chapter 2

4. GAS-LIQUID MASS TRANSFER IN A SLURRY BUBBLE COLUMN REACTOR AT FISCHER-TROPSCH CONDITIONS

4.1 Introduction

The catalytic performance of Fe and $FeRu/SiO_2$ was investigated in a vigorously stirred autoclave in order to eliminate physical transport limitations. However, for the industrial application of the Fischer-Tropsch synthesis in the liquid phase a bubble column type reactor is preferred. Therefore, special attention is given to mass transfer in such a reactor.

The most important transport resistance in bubble column slurry reactors is the mass transfer from gas bubbles to liquid. The rate of the conversion of synthesis gas is first order with respect to the hydrogen pressure, provided the CO conversion level and the H_2/CO inlet ratio are lower than 90% and 1 respectively. Thus particular attention has to be given to the mass transfer of hydrogen.

Before explaining the aim of the experiments presented in this chapter, the scarce amount of literature concerning gas-liquid mass transfer in a Fischer-Tropsch bubble column reactor will be briefly discussed. The extent to which the performance of a Fischer-Tropsch bubble column reactor is limited by this hydrogen transport has been the subject of some discussions recently [1,3,4,5,6,7]. The main subject of this discussion is the length of the mean gas bubble diameter. The calculation of this is hindered by a lack of consistent relations predicting the bubble diameter and specific contact area as function of observable parameters such as power consumption, specific gas load and gas, liquid and solids properties [18].

Furthermore reliable experimental data are scarce. Only Zaidi [9,12] and Hammer [13] have determined values of k_La in a bubble column containing catalyst particles suspended in molten wax. These k_La-values are related to CO. From this data the value of k_La for H_2 can be calculated, although the $k_{L,H_2}/k_{L,CO}$ ratio is also unclear [2,3,4,10,11].

The gas-liquid surface has been measured by Calderbank et al.[14] using a light-transmission method [15] in molten wax, but in the absence of suspended particles. From this report it follows that the mean bubble diameter in a Fischer-Tropsch bubble column is 2.1 mm in the bubble flow regime. The correlation of Deckwer [16] for calculation of the gas-liquid

surface, which is frequently used, reads:

$$a = 4{,}5\ U_{G,O}^{1.1}$$

This correlation is based on values of the gas holdup and photographically determined bubble diameters, which are approximately 0.7 mm in the bubble flow regime [5,8,9]. These bubble diameter measurements were also carried out without the presence of solids.

In view of this lack of experimental data for the value of $k_La_{H_2}$ under Fischer-Tropsch conditions and especially the effect of solids on the value of k_La, it was decided to carry out our own experiments, particulary regarding the influence of catalyst particles and also that of the gas distributor and liquid column height on the value of $k_La_{H_2}$.

Because of the low reaction rate, and the complicated behaviour of the catalyst, a catalytic model reaction for the determination of k_La was selected, rather than the Fischer-Tropsch reaction itself.

The results obtained in this study will be used in the last section to predict the importance of gas-liquid mass transfer to the rate of the Fischer-Tropsch synthesis in a slurry bubble column.

4.2 The resistance in series model

For the determination of the volumetric liquid-side mass transfer coefficient (k_La) one can apply the principle of the "resistance in series" model. In this section the suitability of the graphical determination of k_La is described by plotting the inverse of the reaction rate versus the inverse of the catalyst concentration.

According to this graphical method the k_La-value can be obtained from conversion measurements if the catalyst concentration, and hence the reaction rate, is varied over a sufficiently wide range. Under steady-state conditions and assuming the liquid phase is not mixed, the rate of transport from gas bubbles to liquid is given by

$$r = k_La(C^*_L - C_L) \qquad (4.1)$$

This rate is equal to the rate of transport from the bulk of liquid phase to the catalyst surface

$$r = k_Sa_S(C_L - C_S)(1-\varepsilon_G) \qquad (4.2)$$

and the rate of reaction

$$r = k\,\eta\,C_{cat}\,C_S(1-\varepsilon_G) \tag{4.3}$$

Combining the Eqs.(4.1) - (4.3), in order to eliminate C_L and C_S, the following equation emerges:

$$\frac{C_L^*}{r} = \frac{1}{k_L a} + \frac{1}{k_S\, a_S(1-\varepsilon_G)} + \frac{1}{k\,\eta\,C_{cat}(1-\varepsilon_G)} \tag{4.4}$$

The right hand side of this equation consists of the sum of the gas-liquid mass transfer resistance, the liquid-solid mass transfer resistance and the "chemical" resistance, including pore diffusion limitation.

If catalyst particles are spheres of diameter d_p, than

$$a_S = \frac{6\,C_{cat}}{\rho_S\, d_p} \tag{4.5}$$

Subsituting of Eq.(4.5) into (4.4) gives:

$$\frac{C_L^*}{r} = \frac{1}{k_L a} + \frac{1}{k_o\,(1-\varepsilon_G)} \cdot \frac{1}{C_{cat}} \tag{4.6}$$

wherein

$$\frac{1}{k_o} = \frac{1}{k_S} \cdot \frac{\rho_S d_p}{6} + \frac{1}{k\,\eta} \tag{4.7}$$

Furthermore, if it is assumed that gas bubbles behave as spheres, an assumption which is justified in the homogeneous regime and for non-viscous liquids, the gas bubble interfacial area, a_S, can be calculated as follows:

$$a_S = \frac{6\,\varepsilon_G}{d_b} \tag{4.8}$$

Combining Eq.(4.8) and (4.6) we obtain

$$\frac{C_L^*}{r} = \frac{d_b}{6\,k_L\,\varepsilon_G} + \frac{1}{k_o\,(1-\varepsilon_G)} \cdot \frac{1}{C_{cat}} \tag{4.9}$$

A plot of C_L^*/r versus $1/C_{cat}$ should yield a straight line with the

ordinate intercept representing the gas-liquid mass transfer resistance ($1/k_La$) [9,17]. However, this implies that both d_p, ε_G and k_L are not affected by the catalyst loading. Later on it will be demonstrated that this assumption is only justified at very low catalyst concentrations. It is interesting to note that the value of the slope in Eq.(4.9) depends on the gas holdup. This means that the slope decreases with increasing gas velocity due to an increase of the gas holdup. Naturally the slope will flatten also with an increase of the temperature due to a faster reaction rate.

When one or more parameters on the right hand side of Eq.(4.9) change due to the addition of catalyst particles, a plot of C_L^*/r versus $1/C_{cat}$ will not yield a straight line. The effects of possible changes of ε_G, d_b and k_L on the value of k_La and the shape of the curve will be discussed briefly. We start with the estimation that the value of the gas holdup decreases due to the addition of catalyst particles. At higher catalyst loadings this decrease of the gas holdup can cause an increase of the total resistance instead of the usual, gradual decline as shown in Figure 4.1. In order to construct this figure, it is assumed that the gas holdup decreases linearly with increasing catalyst concentration (which is found experimentally). Thus, at higher catalyst concentration the increase of the $1/k_La$-value is much higher than the decrease of the "chemical resistance". This decrease of the k_La-value may remain unnoticed due to the usual experimental scattering, if the value of k_La is determined on basis of a relatively small range of catalyst concentrations.

In case the mean gas bubble diameter increases due to the addition of solids, naturally this also causes a decrease of the k_La-value. Since a linear increase of the bubble diameter is not likely, it is assumed that the bubble diameter quickly reaches an equilibrium value. When the increase of the bubble diameter depends exponentially on the catalyst concentration a curve as shown in Figure 4.2 will be found. Again it may be noted that this deviation of the normal straight line might not be visible by scattering of the data points.

Finally, catalyst addition may influence the k_L-value and thus k_La as well. In this connection it may be said that this effect on the k_La-value cannot be distinguished from that due to the increase of the bubble diameter if both k_L and d_b change by the addition of catalyst particles.

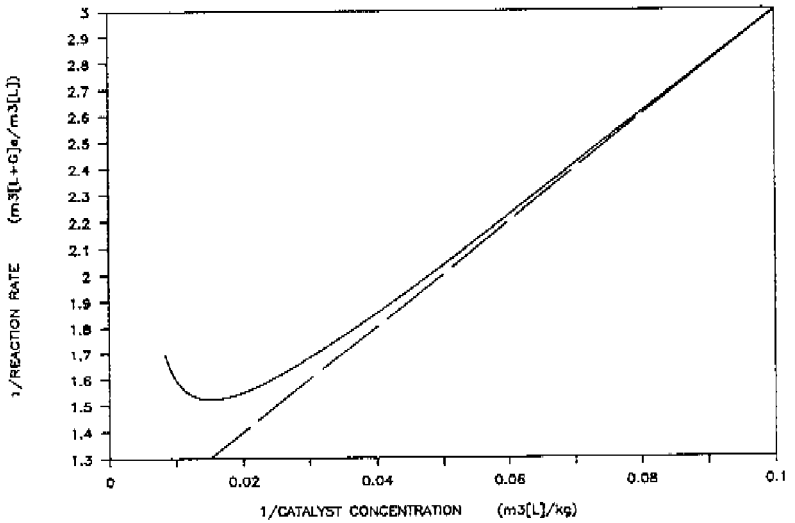

Fig. 4.1 Predicted inverse effective reaction rate as a function of inverse catalyst concentration assuming that only the gas holdup depends on the catalyst concentration. The dashed line represents the situation that all hydrodynamic parameters are independant of the catalyst concentration.

Assumptions:

$k_La = 1.0 \quad (C_{cat} = 0)$ $\quad m^3_L/m^3_{L+G}\ s$

$e_G = 0.322(1-0.00298C_{cat})$ $\quad m^3_G/m^3_{L+G}$

$k_O\eta = 0.074$ $\quad m^3_L/kg_{cat}\ s$

Deviations from the straight line, obtained according to the graphical method (Eq.(4.9)), also emerge when the gas absorption rate is enhanced by the addition of catalyst particles. Two possibilities can be distinguished. The first one is enhancement by an increase of k_L [19,20,21,22,23]. This "shuttle" mechanism or "grazing" model has been proved nearly exclusively for active carbon particles [23], i.e. particles with extremely high specific surface areas. Thus, this type of enhancement is of no importance for other, more common, catalyst materials.

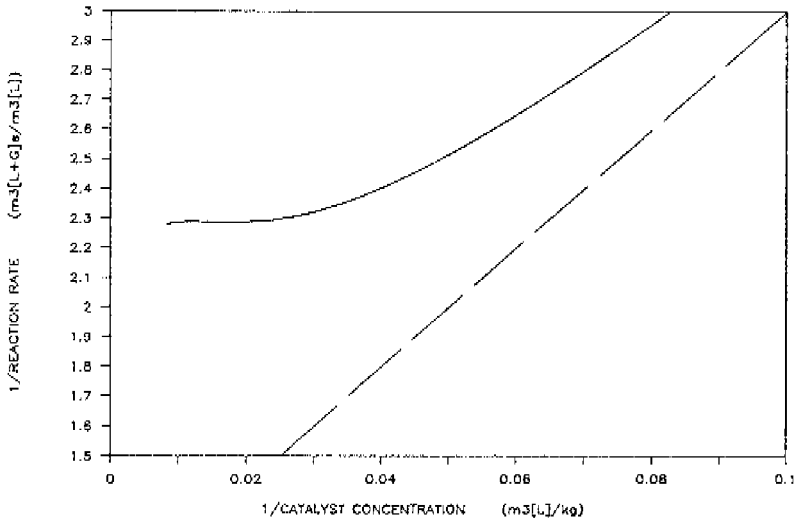

Fig. 4.2 Predicted inverse effective reaction rate as a function of the inverse catalyst concentration assuming that only d_b changes significantly with the catalyst concentration. Assumptions:

$k_La = 1 \quad (C_{cat} = 0)$	$m^3_L/m^3_{L+G}\ s$
$e_G = 0.322$	m^3_G/m^3_{L+G}
$k_on = 0.074$	$m^3_L/kg_{cat}\ s$
$d_b = d_{b,e} - (d_{b,e} - d_{b,C_{cat}=0})\exp(-0,03\ C_{cat})$	m_G
$d_{b,e} = 1.5x10^{-3}$	m_G
$d_{b,C_{cat}=0} = 0.7x10^{-3}$	m_G

The second possibility is enhancement of the gas absorption rate by reaction on catalyst particles in the liquid film around gas bubbles. In that case two conditions must be fulfilled. Firstly, the catalyst particle diameter, d_p, has to be sufficiently small compared to the liquid film thickness, δ, for instance $d_p = 0.1\delta$ [23]. Secondly, the concentration of the gas in the bulk liquid must be approximately zero [24]. It is clear that the second condition is not fulfilled when applying

the graphical method ($C_{H_2,L}>0$). It may be noted that in case the concentration of the gas in the liquid is indeed approximately zero (high catalyst concentration) the catalyst must be extremely active in order to cause a substantial conversion in the liquid film. It can thus be concluded that enhancement of gas absorption will not play a role in this study, in which a common catalyst is used.

Finally, the value of k_La may depend on the concentration of the catalyst particles. In that case, no linear curve is obtained if C_L^*/r is plotted versus 1/m. Nevertheless, this figure can be used for the determination of the order of magnitude of the k_La-value. The influence of the catalyst concentration on the k_La-value cannot be determined by this method.

Therefore, in this study, two procedures have been applied. The first procedure, the graphical method (variation of the catalyst loading), was applied for the determination of the k_La-value at low catalyst concentrations. The second procedure was applied for the determination of k_La at higher solid concentrations. The initial amount of catalyst was high enough to provide that the conversion of H_2 was only determined by the gas-liquid mass transfer resistance. Therefore, a change of the conversion by the addition of catalyst or inert particles could be directly attributed to a change of the k_La-value.

4.3 Calculation of k_La from conversion data

The volumetric mass transfer coefficient k_La of H_2 can be determined applying the graphical method or directly from the conversion of H_2 as pointed out in the previous section. In both cases the behaviour of the gas and liquid phase has to be known. This section describes the relation between the hydrogen conversion, the value of the gas-liquid mass transfer resistance and the chemical resistance for various reactor models. All models are based on the following assumptions:

* the reaction equation is $A + H_2 \rightarrow P$
* the production rate of P, r, is first order in H_2 and independent of the concentration of A : $r = k_o\, C_{H_2,L}$
* the catalyst concentration in the liquid phase is uniform
* the temperatures of the gas, liquid and solid phase are uniform and equal

Model I. Gas phase behaves as plug flow; liquid phase is not mixed

The combination of a tall reactor with respect to the diameter and a rapid reaction results in a concentration profile of hydrogen in the liquid phase over the height of the reactor. The liquid phase can be considered as non-mixed if the reciprocal first order reaction constant is much smaller than the mixing time. Especially for a reactor which is relatively high the mixing may not be sufficiently rapid to prevent a concentration profile in the liquid phase. In that case the mixing of the gas phase occurs probably slowly as well because the mixing of both phases are related. When the gas mixing time is so large that this time is much larger than the gas residence time, the gas phase can be regarded as plug flow. The mass balance of hydrogen over a differential element in this bubble column is then:

$$\frac{-d(U_G\, C_{H_2,G})}{dz} = k_L a(C^*_{H_2,L} - C_{H_2,L}) \qquad (4.10)$$

The reaction rate, r, follows from Eq.(4.4) and is equal to

$$r = k_{ov}\, C^*_{H_2,L} = k_L a(C^*_{H_2,L} - C_{H_2,L}) \qquad (4.11)$$

In this equation $1/k_{ov}$ is the overall resistance, i.e. the sum of the resistances mentioned in Eq.(4.4)
Combination of the Eqs. (4.10) and (4.11) gives:

$$\frac{-d(U_G\, C_{H_2,G})}{dz} = k_{ov}\, \frac{C_{H_2,G}}{m} \qquad (4.12)$$

where m is the solubility coefficient

$$m = \frac{C_{H_2,G}}{C_{H_2,L}} \qquad (4.13)$$

Both gas velocity and hydrogen concentration depend on the conversion of H_2

$$U_G = U_G^{in}(1-f\, X_{H_2}) \qquad (4.14)$$

$$C_G = C_{H_2}^{in},_G\, \frac{(1-X_{H_2})}{(1-f\, X_{H_2})} \qquad (4.15)$$

where f is the H_2 fraction in the inlet gas flow. Finally, after substituting Eqs.(4.15) and (4.16) in Eq.(4.12) and integrating over the height L, the relation between the overall resistance and the conversion of H_2 is obtained:

$$\frac{1}{k_{ov}} = \frac{L_{L+G}}{U_G^{in}\, m_{H_2}(f-1)\ln(1-X_2) + fX_{H_2}} \tag{4.16}$$

The value of k_{ov} is determined experimentally; the value of k_La can be calculated.

Model 2. Gas phase behaves as plug flow; liquid phase is perfectly mixed

A perfectly mixed liquid phase is approached in bubble columns if the chemical reaction is slow compared to the mixing time of the liquid phase. Nevertheless, the mixing time of gas phase can be large relative to the gas residence time, resulting in a plug flow behaviour of the gas phase. The mass balance of H_2 for the gas phase is given by:

$$\frac{-d(U_G\, C_{H_2,G})}{dz} = k_La(C^*_{H_2,L} - C_{H_2,L}) \tag{4.17}$$

Replacing Eqs.(4.13), (4.14) and (4.15) in (4.17) gives

$$U_G^{in}\, C_G^{in} \frac{d\, X_{H_2}}{dz} = k_La\left[\frac{C_G^{in}}{m_{H_2}} \cdot \frac{1-X_{H_2}}{1-f\, X_{H_2}} - C_{H_2,L}\right] \tag{4.18}$$

This equation can be integrated without replacement of C_L because this concentration is constant over the height. Thus, we obtain

$$\int_0^{X_{H_2}} \frac{1 - f\, X_{H_2}}{1 - X_{H_2} - \dfrac{C_{H_2,L}\, m_{H_2}(1-f\, X_{H_2})}{C^{in}_{H_2,G}}} = \int_0^{L_{L+G}} \frac{k_La}{U^{in}_G\, m_{H_2}} \tag{4.19}$$

or

$$\frac{f-1}{\left[1-\frac{f\,C_{H_2,L}\,m_{H_2}}{C^{in}_{H_2,G}}\right]^2}\ln\left[1-\frac{\frac{1-f\,C_{H_2,L}\,m_{H_2}}{C^{in}_{H_2,G}}}{1-\frac{C_{H_2,L}\,m_{H_2}}{C^{in}_{H_2,G}}}.X\right]+\frac{f}{1-\frac{f\,C_{H_2,L}\,m_{H_2}}{C^{in}_{H_2,G}}}.X = \pm\frac{k_L a\,L_{L+G}}{U_G{}^{in}\,m_{H_2}} \qquad (4.20)$$

The unknown C_L in Eq.(4.20) can be written in terms of conversion with the help of the following mass balances:

$$r = k_S\,a_S\,(C_{H_2,L}-C_{H_2,S})(1-\varepsilon_G) \qquad (4.21)$$

$$r = k\,\eta\,C_{cat}\,C_{H_2,S}\,(1-\varepsilon_G) \qquad (4.22)$$

$$r = U_G{}^{in}\,A\,C^{in}_{H_2,G}\,X_{H_2}/V_{L+G} \qquad (4.23)$$

After combining Eqs. (4.21), (4.22), (4.23), and (4.7), the following equation is obtained:

$$C_L = \frac{U_G{}^{in}C_G{}^{in}\,X_{H_2}}{k_o\,C_{cat}\,L_{L+G}(1-\varepsilon_G)} \qquad (4.24)$$

Finally, on replacing Eq.(4.24) in Eq.(4.20) and introducing the dimensionless parameters

$$N_m = k_L a\,\frac{L_{L+G}}{m\,U_G{}^{in}} \qquad (4.25)$$

and

$$N_r = k_o\,C_{cat}(1-\varepsilon_G)\,\frac{L_{L+G}}{m\,U_G{}^{in}} \qquad (4.26)$$

the following equation is obtained:

$$\frac{f-1}{\left[1-\frac{f\,X_{H_2}}{N_r}\right]^2}\ln\left[1-\frac{1-\frac{f\,X_{H_2}}{N_r}}{1-\frac{X_{H_2}}{N_r}}.X_{H_2}\right]+\frac{f\,X_{H_2}}{1-\frac{f\,X_{H_2}}{N_r}} = N_m \qquad (4.27)$$

Clearly, the value of k_La cannot be determined by way of the method indicated in Eq.(4.9). This is only possible for the special case where the contraction of the gas phase is neglible (low value of f), in which case Eq.(4.27) can be simplified and written as follows:

$$\frac{1}{X_{H_2}} = \frac{1}{1 - \exp\left[- k_La \frac{L_{L+G}}{m_{H_2} U_G^{in}} \right]} + \frac{U_G^{in} m}{k_o L_{L+G}(1-\varepsilon_G)} \cdot \frac{1}{C_{cat}} \qquad (4.28)$$

The value of k_La can be found via a similar method as given in section 4.2. Thus, when 1/X is plotted versus $1/C_{cat}$, a straight line should arise, provided the conditions reported in section 4.2 are fulfilled. The value of k_La and the reaction rate constant can be determined from the intersection on the ordinate and slope respectively.

Model 3 Gas and liquid phase behave as two mixed reactors in series

The last model is based on the assumption that the reactor can be described as two mixed reactors in series (see Figure 4.3).
The mass balances for the first mixed reactor are

$$U_G^0 C^0_{H_2,G} - U_G^1 C^1_{H_2,G} = k_La(C^1_{H_2,G}/m - C^1_{H_2,L})\tfrac{1}{2}V_{L+G} \qquad (4.29)$$

$$k_La(C^1_{H_2,G}/m - C^1_{H_2,L})\tfrac{1}{2}V_{L+G} = k_Sa_S(C^1_{H_2,L} - C^1_{H_2,S})\tfrac{1}{2}V_{L+G}(1-\varepsilon_G) \qquad (4.30)$$

$$k_Sa_S(C^1_{H_2,L} - C^1_{H_2,S})\tfrac{1}{2}V_{L+G}(1-\varepsilon_G) = k\, n\, C_{cat}\, C^1_{H_2,S}\tfrac{1}{2}V_{L+G}(1-\varepsilon_G) \qquad (4.31)$$

By combining Eqs. (4.29), (4.30), and (4.31) Eq.(4.32) is obtained

$$U^0_G C^0_{H_2,G} - U^1_G C^1_{H_2,G} = k_{ov} C^1_{H_2,G}\tfrac{1}{2}L_{L+G}/m \qquad (4.32)$$

For the second mixed reactor Eq.(4.33) is obtained similarly

$$U^1_G C^1_{H_2,G} - U^2_G C^2_{H_2,G} = k_{ov} C^2_{H_2,G}\, \tfrac{1}{2} L_{L+G}/m \qquad (4.33)$$

Replacing Eq.(4.32) in (4.33), then rearranging, Eq.(4.34) is obtained in which the conversion is expressed:

$$1 - X_{H_2} = \frac{U^1_G + U^2_G}{(U^1_G + k_{ov}\tfrac{1}{2}L_{L+G}/m)(U^2_G + k_{ov}\tfrac{1}{2}L_{L+G}/m)} \qquad (4.34)$$

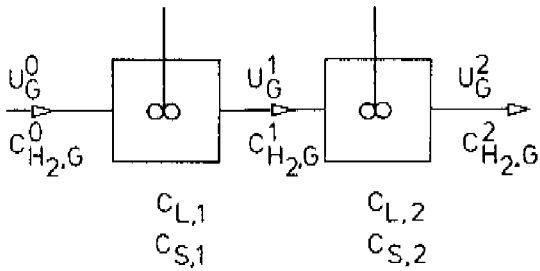

Fig. 4.3 Diagram of model 3

The gas velocities U_G^1 and U_G^2 in this equation are dependent on the conversion. Therefore, k_{ov} cannot be written as a function of X. In the case the gas contraction is negligible ($U_G^1 = U_G^2 = U_G$), Eq.(4.34) can be reduced to:

$$\frac{1}{k_{ov}} = \frac{\frac{1}{2}L_{L+G}}{m_{H_2}\, U_G} \cdot \frac{(1-X_H)^{\frac{1}{2}}}{1-(1-X_{H_2})^{\frac{1}{2}}} \qquad (4.35)$$

Knowing the values of k_{ov} from measured conversion data, the value of k_La can be calculated.

4.4 Choice of the reactor models

The models which have been used for calculating the overall resistance from the conversion are chosen on account of calculated values of the mixing time of the liquid, t_m, the number of mixing cells for the gas phase and experimental determined values of the reaction time t_r.

The mixing time of the liquid is calculated according to [43]:

$$t_m = 3.75\, \varepsilon_G \frac{D_r^{2/3}}{U_G} \left[1 - 0.174\left[\frac{L_{L+G}}{D_r} - 1\right] + 0.17\left[\frac{L_{L+G}}{D_r} - 1\right]^2\right] \qquad (4.36)$$

The characteristic reaction time, t_r, simply follows from the experiments

$$t_r = \frac{1}{k_o\, m} \qquad (4.37)$$

The number of mixing cells for the gas phase are calculated from the Bodenstein number [44]

$$\frac{1}{n} = \frac{2\,[Bo - 1 + \exp(-Bo)]}{Bo^2} \qquad (4.38)$$

wherein $Bo = \dfrac{U_G^0\, L_{L+G}}{D_G\, \varepsilon_G}$

For the calculation of the Bo-number the dispersion coefficient of the gas phase must be known. This dispersion coefficient has been calculated according to the correlation of Mangartz and Pilhofer [42]

$$D_G = 5 \times 10^{-4}\, \frac{U_G^{\,3}}{\varepsilon_G^{\,3}}\, D_r^{1.5} \qquad (4.39)$$

With help of the relations mentioned above, the behaviour of the gas and liquid phase are estimated for the bubble column used, having an inner diameter of 5 cm. The reactor models chosen for four experimental situations are shown in Table 4.1. The choice has been made on the base of reaction time, number of mixing cells and mixing time. The models 2

Table 4.1

Calculated liquid mixing times, numbers of mixing cells of the gas phase and reaction times for four experimental situations. The superficial gas velocity varies from 2-5 cm/s.

Distributor	L/D_r [-]	t_m [s]	n_G [-]	t_r [s]	Chosen models liquid	gas	no.
perforated	2½	1-2	1½-2½	2-4	2 mixing cells	2 mixing cells	3
perforated	20	> 160	> 10	4-20	non-mixed	plug flow	1
porous	2½	4-6	> 6	1-20	mixed	plug flow	2
porous	20	> 240	> 40	2-40	non-mixed	plug flow	1

and 3 have been chosen at low L/D_r ratio (2%). When this ratio exceeded the value of 5, model 1 was used. Using the porous plate at a low L/D_r ratio (2%), the reaction time was longer than the mixing time when the catalyst loading was low. Although the opposite was the case for a higher loading, model 2 was used because the situation at lower catalyst concentrations is the most important as than the graphical method was applied.It should be borne in mind that the degree of mixing at high catalyst concentrations is less important because the hydrogen concentration then approaches zero. The gas flow for this case (second line from the bottom in Table 4.1) is supposed to be plug flow. It should be noted that the difference of the degree of mixing between the perforated and porous plate is caused by the difference in gas holdup as will be shown later.

4.5 Choice of the model reaction

A simple reaction for measuring the gas-liquid mass transfer resistance of hydrogen is more appropriate than the Fischer-Tropsch synthesis itself since the latter reaction is very complex and perhaps too slow for accurate determination of the volumetric mass transfer coefficient. Such a catalytic model reaction must comply with a number of conditions. The main ones are:

* (pseudo) first order in hydrogen
* high reaction rate
* applicable at 300°C

The requirements concerning the catalyst are:

* stable up to 300°C
* selective
* non-coagulating

A suitable reaction appeared to be the hydrogenation of ethene catalysed by palladium on alumina. This system complies with the conditions mentioned above provided that the inlet ethene and hence is at least 97%. The liquid phase can then be regarded as saturated with ethene and the reaction rate then depends on the hydrogen pressure only. The activity of the catalyst is so high that a few weight percent is enough to reduce the hydrogen concentration in the liquid phase to practically zero. The only drawback of this catalyst is the formation of foam in case of low